Enhancement of Breakdown Voltage in AlGaN/GaN HEMTs: Field Plate Plus High-*k* Passivation Layer and High Acceptor Density in Buffer Layer

Toshiki Kabemura, Shingo Ueda, Yuki Kawada, and Kazushige Horio, *Senior Member, IEEE*

***Abstract*— We make a 2-D analysis of breakdown characteristics of field-plate AlGaN/GaN HEMTs with a high-*k* passivation layer, and the results are compared with those having a normal SiN passivation layer. As a result, it is found that the breakdown voltage is enhanced particularly in the cases with relatively short field plates because the reduction in the electric field at the drain edge of gate effectively improves the breakdown voltage in the case with the high-*k* passivation layer. In the case with the moderate-length field plate, the enhancement of breakdown voltage due to the high-*k* passivation layer occurs because the electric field profiles between the field-plate edge and the drain become more uniform. It is also studied how the breakdown voltage depends on a deep-acceptor density in the Fe-doped semi-insulating buffer layer when a high-*k* passivation layer is used. It is shown that the breakdown voltage increases with increasing the relative permittivity of the passivation layer ε_r and with increasing the deep-acceptor density N_{DA}. When $\varepsilon_r = 60$ and $N_{DA} = 2\text{–}3 \times 10^{17}$ cm^{-3} at the gate length of 0.3 μm, the breakdown voltage becomes about 500 V at a gate-to-drain distance of 1.5 μm, which corresponds to an average electric field of about 3.3 MV/cm between the gate and the drain.**

***Index Terms*— 2-D analysis, breakdown characteristics, buffer layer, GaN HEMT, high-k passivation layer.**

I. Introduction

NOWADAYS, AlGaN/GaN HEMTs are attractive for applications to high-power microwave devices and high-power switching devices [1], [2]. It is well known that introducing a field plate enhances the power performance of AlGaN/GaN HEMTs as well as GaAs FETs [3]–[5]. This occurs because by introducing a field plate, the current collapse is reduced [6], [7], and the breakdown voltage increases [8]–[10]. The increase in breakdown voltage occurs because the electric field at the drain edge of gate is reduced by introducing a field plate.

Manuscript received April 17, 2018; revised May 30, 2018 and June 17, 2018; accepted July 17, 2018. Date of publication July 31, 2018; date of current version August 21, 2018. This work was supported by JSPS KAKENHI under Grant JP16K06314. The review of this paper was arranged by Editor K. J. Chen. *(Corresponding author: Kazushige Horio.)*

The authors are with the Faculty of Systems Engineering, Shibaura Institute of Technology, Saitama 337-8570, Japan (e-mail: horio@sic.shibaura-it.ac.jp).

Color versions of one or more of the figures in this paper are available online at http://ieeexplore.ieee.org.

Digital Object Identifier 10.1109/TED.2018.2857774

To increase the breakdown voltage in AlGaN/GaN HEMTs, the introduction of the passivation layer with high permittivity (high-*k* layer) is also considered [11]–[13]. Introducing a high-*k* material may smooth the electric field profiles between the gate and the drain [11]. The high-*k* material is investigated as a gate insulator in AlGaN/GaN MISHEMTs [14]–[16], for example, HfO_2 (relative permittivity $\varepsilon_r \sim 20$), La_2O_3 ($\varepsilon_r \sim 27$), $LaLuO_3$ ($\varepsilon_r \sim 28$), and TiO_2 ($\varepsilon_r \sim 55$) are studied [14]–[16]. In [12] and [13], the high-*k* material was considered only as a passivation layer, and we calculated the OFF-state breakdown characteristics in AlGaN/GaN HEMTs as a parameter of ε_r. It was shown that the breakdown voltage increased as ε_r increased because the electric field at the drain edge of gate was reduced. It is also shown that when the gate voltage is more negative, the breakdown voltage is improved in the high ε_r region because the buffer leakage current is reduced [17].

In this paper, we combine the two structures and analyze the breakdown characteristics of field-plate AlGaN/GaN HEMTs with a high-*k* passivation layer, and the results are compared with those having a normal SiN passivation layer. We investigate how the breakdown voltage is changed by the field-plate length and the relative permittivity of the passivation layer. We also study the breakdown characteristics of AlGaN/GaN HEMTs with a Fe-doped semi-insulating buffer layer, where the deep-acceptor (Fe) density is varied. The deep-acceptor density may affect the buffer leakage current, and hence it should change the breakdown voltages of AlGaN/GaN HEMTs.

In Section II, we describe physical models used here, such as a device structure, buffer-trap models, and basic equations for the device analysis. In Section III, calculated OFF-state breakdown characteristics of field-plate AlGaN/GaN HEMTs with different permittivities in the passivation layer are described. In Section IV, the dependence of breakdown characteristics on the deep-acceptor density in the Fe-doped semi-insulating buffer layer is described. Finally, the conclusion is given in Section V.

II. Physical Models

Fig. 1 shows a device structure analyzed in this paper. The gate length L_G is 0.3 μm, the source-to-gate distance L_{SG}

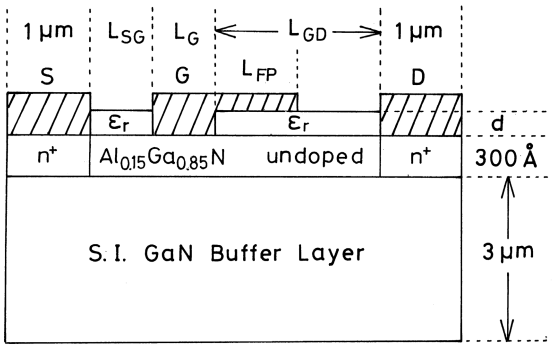

Fig. 1. Device structure analyzed in this paper.

is 0.5 μm, and the gate-to-drain distance L_{GD} is 1.5 μm. The thickness of the passivation layer d is 0.1 μm. The field-plate length L_{FP} is varied between 0 and 1 μm. The relative permittivity of the passivation layer ε_r is varied between 1 and 60. Here, we do not consider the dynamics of passivation layer/AlGaN barrier interface states. According to our simulation on GaAs MESFETs [18], when the dominant interface states act as electron traps, the drain voltage is almost applied along the drain edge of the gate, which is similar to the case without interface states. When they act as hole traps, the drain voltage is almost applied along the gate edge of the drain. So, if the situation is former, the results obtained here may become similar to the case of considering trapping effects. In a semi-insulating buffer layer, we usually consider a shallow donor, a deep donor, and a deep acceptor [19]–[21]. The shallow-donor density N_{Di} is set to 10^{15} cm^{-3}. As an energy level of the deep acceptor, we consider $E_C - 2.85$ eV ($E_V + 0.6$ eV). For impurity compensation, we consider the deep donor whose energy level is $E_C - 0.5$ eV. The deep-acceptor density N_{DA} is set rather high of 10^{17} cm^{-3}. According to [22], the acceptor density in a buffer layer should be higher than 10^{17} cm^{-3} to suppress the short-channel effects in AlGaN/GaN HEMTs. The buffer layer is set floating here. If the buffer layer or a substrate is grounded, the vertical current may flow from the drain to the substrate. However, the trap-filled limit voltage is estimated to be about 850 V at $N_{DA} = 10^{17}$ cm^{-3}. This is rather higher than the breakdown voltages estimated here ($\leq$500 V). So, the estimated breakdown voltage may not be so changed. In Section IV, we consider a Fe-doped semi-insulating buffer layer, where only a deep acceptor above the midgap is considered. Here, the deep-acceptor's energy level is set to $E_C - 0.5$ eV [23], [24]. The deep-acceptor density N_{DA} is varied between 10^{17} and 3×10^{17} cm^{-3}. At higher acceptor densities ($>3 \times 10^{17}$ cm^{-3}), obtaining convergence in the numerical analysis becomes sometimes difficult, and comprehensive results to show are not obtained.

Basic equations to be solved are Poisson's equation including ionized deep-level terms and continuity equations for electrons and holes including a carrier generation rate by impact ionization and carrier loss rates via the deep levels [10], [13], [18], [25]. These are expressed as follows.

1) *Poisson's equation:*

$$\nabla \bullet (\varepsilon \nabla \psi) = -q(p - n + N_{Di} + N_{DD}^{+} - N_{DA}^{-}). \quad (1)$$

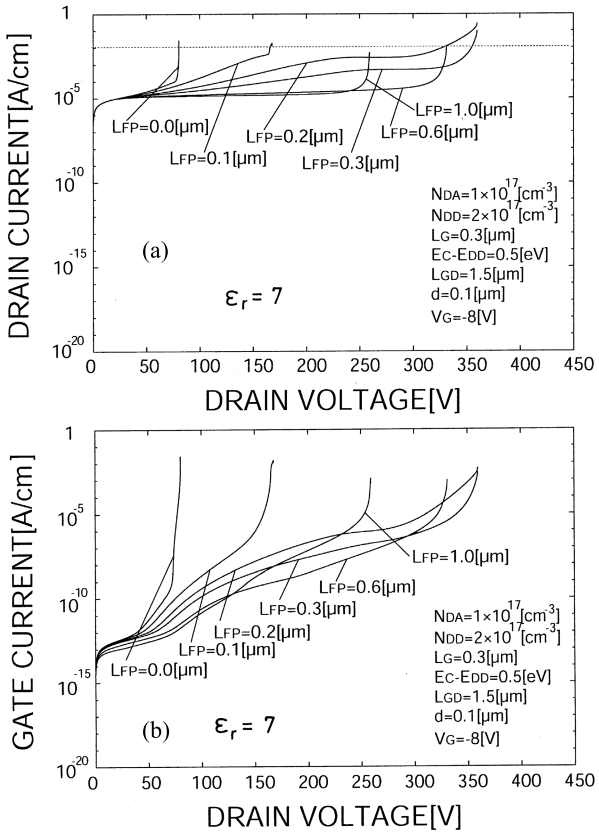

Fig. 2. Calculated (a) I_D–V_D curves and (b) I_G–V_D curves as a parameter of L_{FP}. $\varepsilon_r = 7$ and $V_G = -8$ V. Dotted lines: 1 mA/mm.

2) *Continuity equations for electrons and holes:*

$$\nabla \bullet J_n = -qG + q(R_{DD} + R_{DA}) \quad (2)$$

$$\nabla \bullet J_p = qG - q(R_{DD} + R_{DA}) \quad (3)$$

where N_{DD}^{+} and N_{DA}^{-} are the ionized deep-donor density and deep-acceptor density, respectively. R_{DD} and R_{DA} are the carrier loss rates via the deep donors and deep acceptors, respectively. G is a carrier generation rate by impact ionization and given by

$$G = (\alpha_n |J_n| + \alpha_p |J_p|)/q \quad (4)$$

where α_n and α_p are the electron and hole ionization rates, respectively, and expressed as

$$\alpha_n = A_n \exp(-B_n/|E|) \quad (5)$$

$$\alpha_p = A_p \exp(-B_p/|E|). \quad (6)$$

Here, E is the electric field. Coefficients A_n, B_n, A_p, and B_p are fitting parameters, and deduced from [26], as in [10] and [13]. Equations (1)–(6) are solved numerically in 2-D.

III. Field Plate Plus High-k Passivation

Figs. 2(a) and (b) shows calculated drain current I_D–drain voltage V_D curves and gate current I_G–V_D curves, respectively, for AlGaN/GaN HEMTs having a SiN passivation layer (relative permittivity $\varepsilon_r = 7$), with the field-plate length L_{FP} as a parameter. Figs. 3(a) and (b) shows calculated I_D–V_D curves

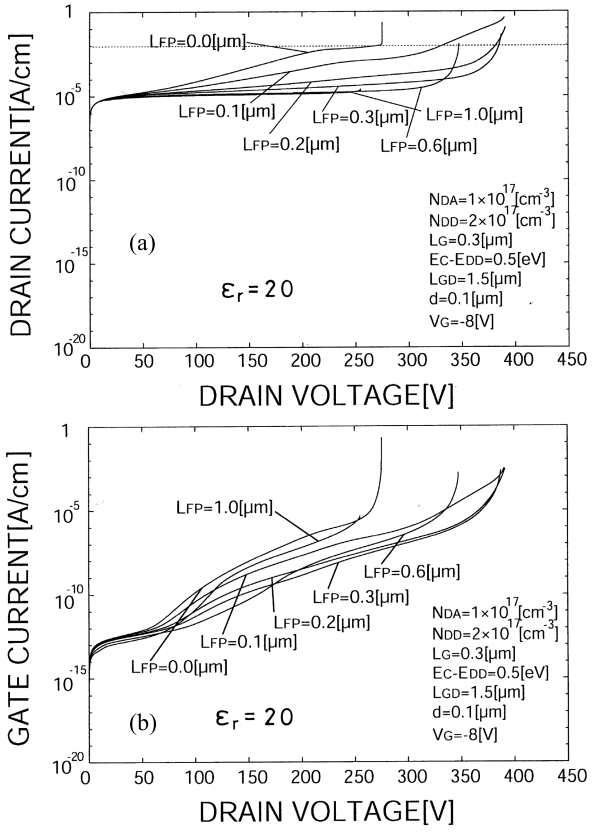

Fig. 3. Calculated (a) I_D–V_D curves and (b) I_G–V_D curves as a parameter of L_{FP}. $\varepsilon_r = 20$ and $V_G = -8$ V. Dotted lines: 1 mA/mm.

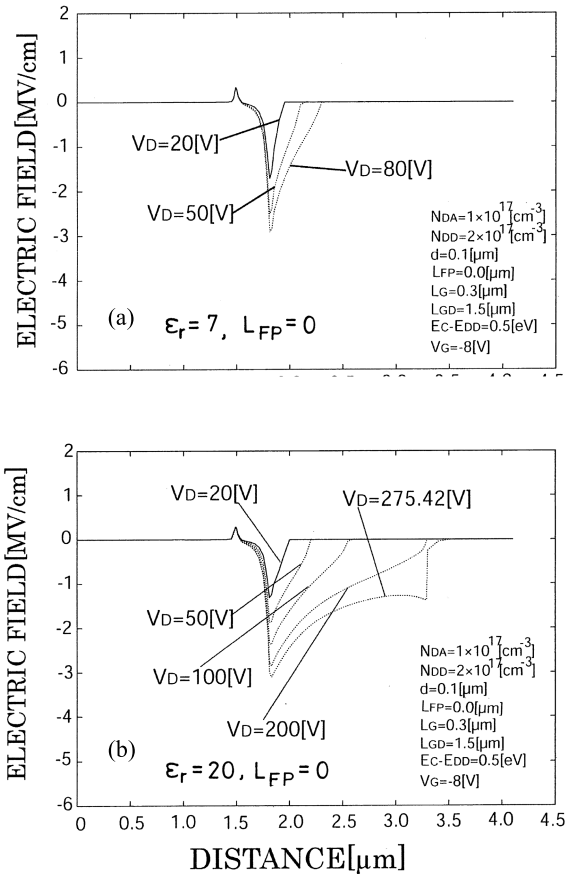

Fig. 4. Electric field profiles along the heterojunction interface. $L_{FP} = 0$. (a) $\varepsilon_r = 7$. (b) $\varepsilon_r = 20$.

and I_G–V_D curves, respectively, for AlGaN/GaN HEMTs with a high-k passivation layer ($\varepsilon_r = 20$), with L_{FP} as a parameter. In both cases, the gate voltage V_G is -8 V, which corresponds to an OFF state. In the cases of $L_{FP} = 0$ in Figs. 2 and 3 and $L_{FP} = 0.1$ μm in Fig. 2, the drain current increases suddenly, showing breakdown. In these cases, the drain current becomes equal to the gate current in the region where the currents increase suddenly. These are considered to occur due to the impact ionization of carriers at the drain edge of gate. In other cases, the drain current usually increases more gradually but steeply [except for $\varepsilon_r = 20$ and $L_{FP} = 0.1$ μm in Fig. 3(a)]. These are also considered as the breakdown. In these cases, the gate current is lower than the drain current by over 1 order of magnitude in the region where the currents increase steeply. Then, the source current becomes nearly equal to the drain current. Therefore, it is considered that in these cases, holes generated by impact ionization between the field-plate edge and the drain flow into the buffer layer as well as into the gate and are captured by the deep donors that determine the Fermi level, lowering the barrier at the source side in the buffer and increasing the buffer leakage current. Overall, the breakdown voltage seems to be higher in the case of $\varepsilon_r = 20$. Particularly, it is higher at relatively short L_{FP}.

Fig. 4 shows a comparison of electric field profiles at the AlGaN/GaN heterojunction interface for $L_{FP} = 0$ between the two cases with $\varepsilon_r = 7$ and 20. In the case of $\varepsilon_r = 7$, the increase in the drain voltage is entirely applied along the drain edge of gate, leading to the breakdown at about 80 V as shown in Fig. 2. On the other hand, in the case of $\varepsilon_r = 20$, the electric field at the drain edge of gate is reduced. As V_D increases, the high electric field region extends toward the drain. Finally, the peak of the electric field at the drain edge of gate becomes ~3 MV/cm around $V_D = 275$ V, which corresponds to the breakdown voltage as shown in Fig. 3.

Fig. 5 shows a comparison of electric field profiles at the AlGaN/GaN heterojunction interface for $L_{FP} = 0.1$ μm between the two cases with $\varepsilon_r = 7$ and 20. In the case of $\varepsilon_r = 7$, the reduction in the electric field at the drain edge of gate is not so significant although the peak of the electric field at the drain edge of gate is lower than ~3 MV/cm at $V_D = 100$ V. In this case, the breakdown occurs at $V_D \sim 167$ V, as shown in Fig. 2. On the other hand, in the case of $\varepsilon_r = 20$, the electric field at the drain edge of gate is greatly reduced, and it does not reach ~3 MV/cm even at $V_D = 390$ V. Rather, in this case, as shown in Fig. 3(a), the drain current does not show an abrupt increase but increases gradually to reach a critical value (1 mA/mm). Here, the buffer leakage current determines the breakdown voltage.

Fig. 6 shows the breakdown voltage as a function of the field-plate length L_{FP}, with ε_r as a parameter. Four cases with different ε_r (7, 20, 30, and 50) are shown. Here, the breakdown voltage is defined as a drain voltage when the drain current becomes 1 mA/mm. It is seen that the breakdown voltage becomes higher when ε_r becomes higher, particularly in the

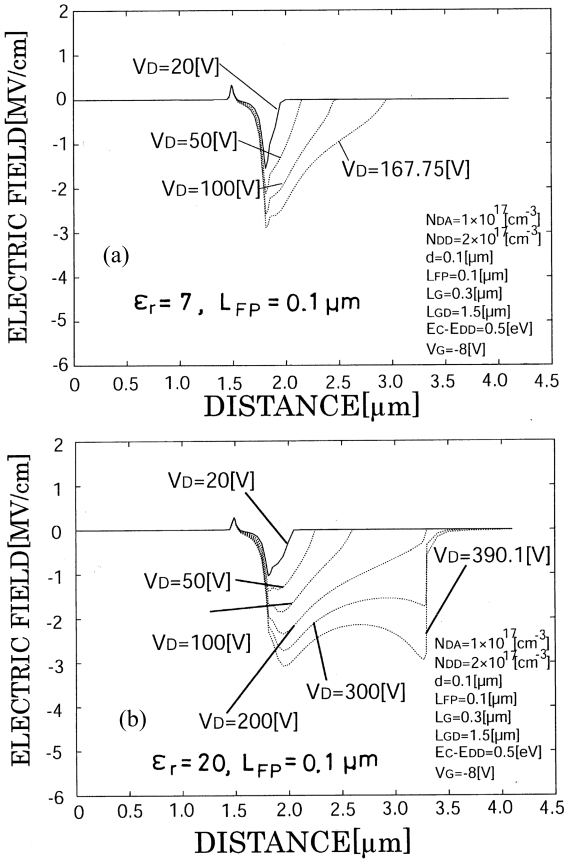

Fig. 5. Electric field profiles along the heterojunction interface. $L_{FP} = 0.1$ μm. (a) $\varepsilon_r = 7$. (b) $\varepsilon_r = 20$.

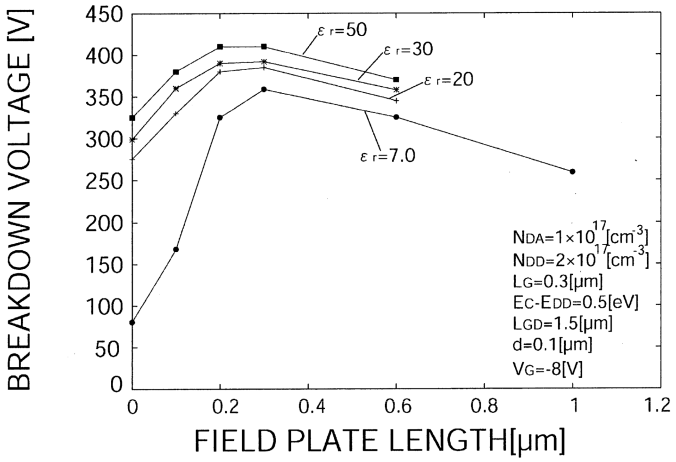

Fig. 6. Breakdown voltage versus field-plate length L_{FP} curves, with ε_r as a parameter.

region where L_{FP} is relatively short. This is favorable because when L_{FP} becomes long, the parasitic capacitance becomes high particularly for high ε_r. From Fig. 6, it is seen that the breakdown voltage becomes low when L_{FP} becomes relatively long (0.6–1 μm). This is because $L_{GD} = 1.5$ μm here, and hence the distance between the field-plate edge and the drain becomes very short. So, the electric field in this region becomes very high, leading to the breakdown [10]. Therefore, there is an optimum field-plate length to obtain

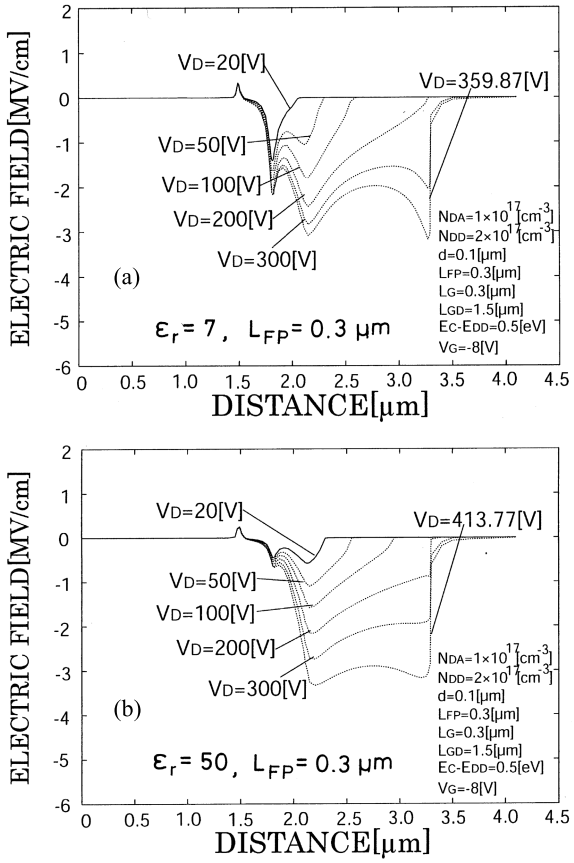

Fig. 7. Electric field profiles along the heterojunction interface. $L_{FP} = 0.3$ μm. (a) $\varepsilon_r = 7$. (b) $\varepsilon_r = 50$.

a high breakdown voltage, and it is around 0.2 and 0.3 μm here. When $\varepsilon_r = 50$ and $L_{FP} = 0.2$ or 0.3 μm, the breakdown voltage becomes over 400 V, which corresponds to an average electric field of about 2.8 MV/cm between the gate and the drain.

Fig. 7 shows a comparison of electric field profiles at the AlGaN/GaN heterojunction interface for $L_{FP} = 0.3$ μm between the two cases with $\varepsilon_r = 7$ and 50. In both cases, the electric field at the drain edge of gate is reduced significantly, and it does not determine the breakdown voltage. It is determined by the electric field profiles between the field-plate edge and the drain.

In the case of $\varepsilon_r = 7$, the electric fields at the drain-electrode edge as well as at the field-plate edge become very high, and these determine the breakdown voltage (~360 V). On the other hand, in the case of $\varepsilon_r = 50$, the electric field profiles in this region are more uniform. This is due to the high-k dielectric, and hence the breakdown voltage becomes higher (~414 V) than that for lower ε_r.

IV. Effects of Acceptor Density in a Buffer Layer

Next, we describe the case with a Fe-doped semi-insulating buffer layer where a deep acceptor above the midgap is considered [27], [28]. Here, we study the dependence of breakdown characteristics on the deep-acceptor density in the buffer layer N_{DA} and the relative permittivity of the passivation layer ε_r. Here, the field-plate length $L_{FP} = 0$.

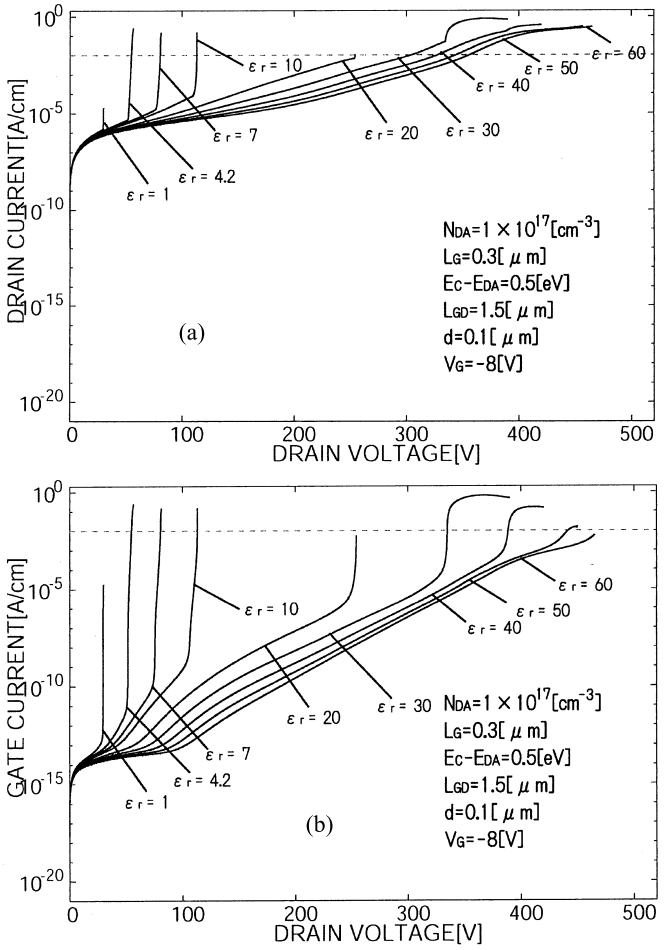

Fig. 8. Calculated off-state (a) I_D–V_D curves and (b) I_G–V_D curves when $N_{DA} = 10^{17}$ cm^{-3}. Dashed lines: 1 mA/mm.

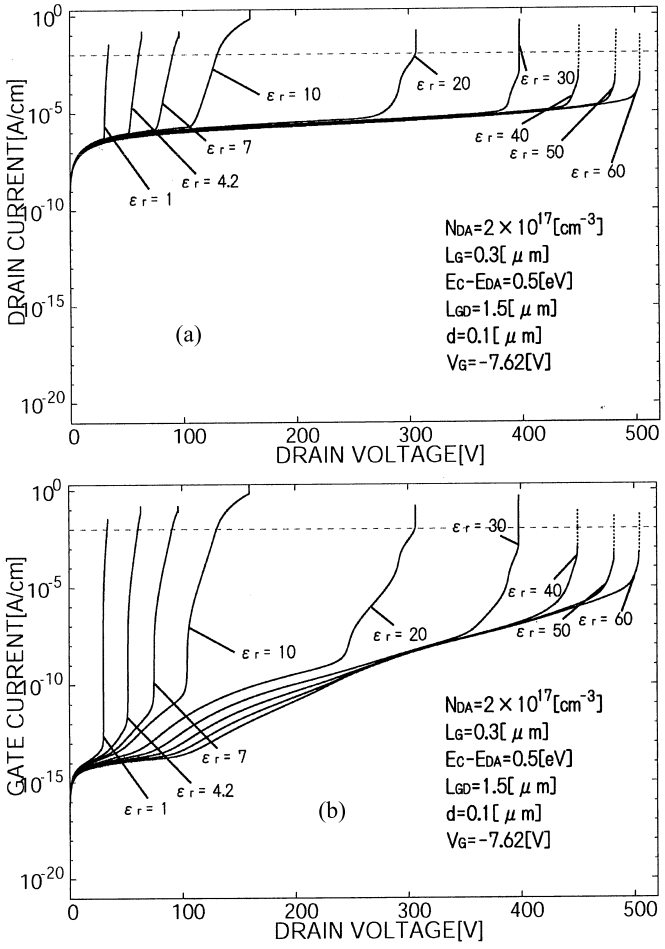

Fig. 9. Calculated off-state (a) I_D–V_D curves and (b) I_G–V_D curves when $N_{DA} = 2 \times 10^{17}$ cm^{-3}. Dashed lines: 1 mA/mm.

Figs. 8 and 9 show calculated I_D–V_D curves [Figs. 8(a) and 9(a)] and I_G–V_D curves [Figs. 8(b) and 9(b)] of AlGaN/GaN HEMTs with a Fe-doped semi-insulating buffer layer as a parameter of relative permittivity of the passivation layer ε_r, where the deep-acceptor densities in the buffer layer N_{DA} are 10^{17} and 2×10^{17} cm^{-3}, respectively. In Fig. 8, where N_{DA} is 10^{17} cm^{-3}, the threshold voltages V_{th} are about -6 V, and the gate voltage is set to $V_G = V_{th} - 2$ V $= -8$ V as in the cases in Section III. Here, the threshold voltage is defined as a gate voltage when I_G becomes 5×10^{-3} A/cm at $V_D = 40$ V. In the case of Fig. 9 where $N_{DA} = 2 \times 10^{17}$ cm^{-3}, V_{th} becomes about -5.62 V for $\varepsilon_r = 7$, and hence V_G is set to $V_{th} - 2$ V $= -7.62$ V. It is seen that in both cases, when ε_r is low ($\leq$10), a sudden increase in drain current occurs due to the impact ionization of carriers, and this determines the breakdown voltage. In the region where I_D increases suddenly, the drain current becomes equal to the gate current. In the case of $N_{DA} = 10^{17}$ cm^{-3}, when ε_r becomes high ($\geq$30), the drain current increases gradually and reaches a critical value (1 mA/mm) before a sudden increase in I_D. In this region, the drain current is much higher than the gate current, and hence the buffer leakage current determines the breakdown voltage at $\varepsilon_r \geq 30$. Note that the breakdown voltage is defined here as the drain voltage when I_D becomes 1 mA/mm. In Figs. 8 and 9, the breakdown voltage increases as ε_r increases. This is because the electric field at the drain edge of gate is reduced when ε_r becomes high [28], as is similarly shown in Fig. 4. In the case of $N_{DA} = 2 \times 10^{17}$ cm^{-3}, even if ε_r becomes high ($\geq$30), the drain current increases suddenly due to the impact ionization of carriers and I_D is nearly equal to I_G in this region. It is understood that in the case of $N_{DA} = 2 \times 10^{17}$ cm^{-3}, the buffer leakage current is reduced due to a steeper barrier at the channel–buffer interface [29]. The dotted lines for $\varepsilon_r = 40$, 50, and 60 indicate extrapolated current–voltage curves where convergence is not obtained.

Fig. 10 shows a comparison of the breakdown voltage versus ε_r curves among the three cases with different N_{DA}. The dotted lines indicate that the convergence is not obtained until $I_D = 1$ mA/mm, and the breakdown voltage is obtained as an extrapolated value as shown in Fig. 9. In the case of $N_{DA} = 2 \times 10^{17}$ and 3×10^{17} cm^{-3}, the breakdown voltages become much higher than that for $N_{DA} = 10^{17}$ cm^{-3} when ε_r becomes higher than 30. This is because the buffer leakage currents become smaller for $N_{DA} = 2 \times 10^{17}$ and 3×10^{17} cm^{-3} and the breakdown voltages become determined by the impact ionization of carriers. In the case of $\varepsilon_r = 60$, the breakdown voltage reaches about 500 V, which corresponds to an average

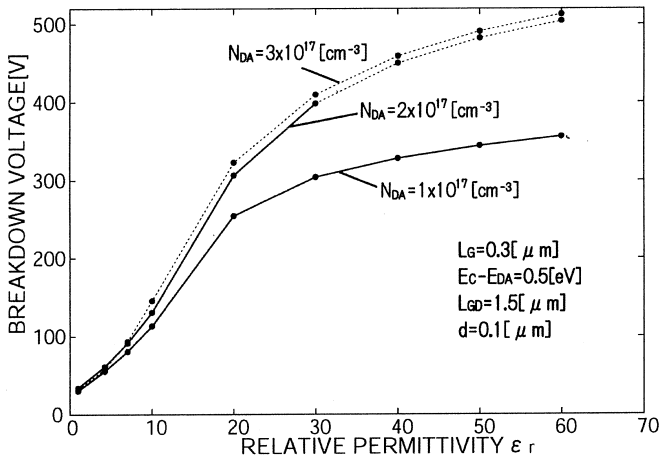

Fig. 10. Comparison of breakdown voltage versus ε_r curves among the three cases with different N_{DA}.

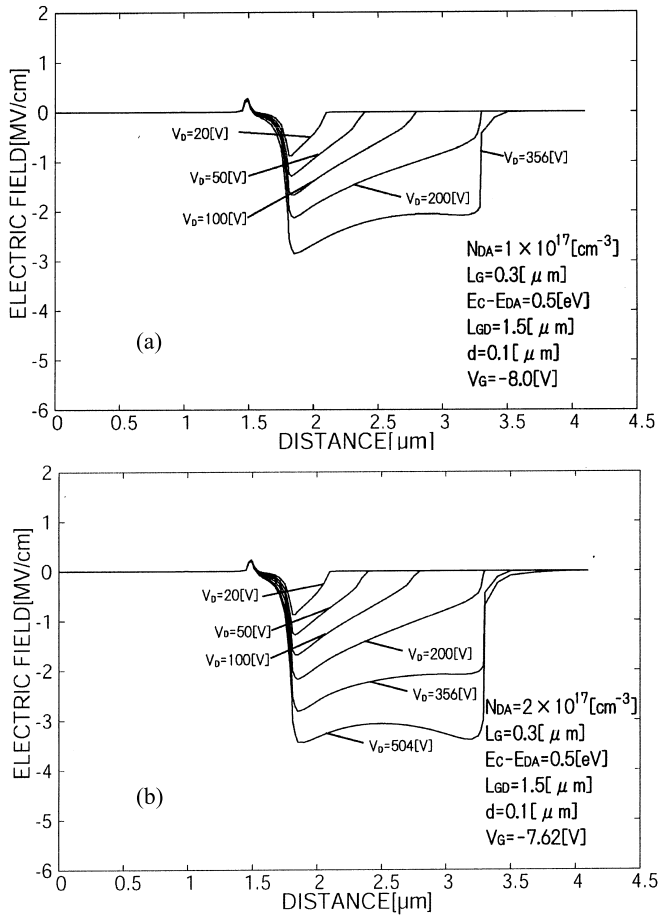

Fig. 11. Comparison of electric field profiles along the heterojunction interface. $\varepsilon_r = 60$. (a) $N_{DA} = 10^{17}$ cm^{-3}. (b) $N_{DA} = 2 \times 10^{17}$ cm^{-3}.

electric field of about 3.3 MV/cm between the gate and the drain. Here, it should be noted that when N_{DA} becomes higher, the so-called current collapse becomes higher due to the trapping effects [29]. Therefore, there is a tradeoff relation between the breakdown voltage and the current collapse.

Fig. 11 shows a comparison of electric field profiles at the AlGaN/GaN heterojunction interface between the two cases with $N_{DA} = 10^{17}$ and 2×10^{17} cm^{-3}. Here, ε_r is 60. The electric field profiles are similar between the two cases until $V_D = 356$ V which is the breakdown voltage for $N_{DA} = 10^{17}$ cm^{-3}, and it is determined by the buffer leakage current. In the case of $N_{DA} = 2 \times 10^{17}$ cm^{-3}, the breakdown voltage is 504 V which is determined by the impact ionization of carriers at the drain edge of gate or at the gate edge of drain. The electric field profiles between the gate and the drain are rather uniform in this case. It is concluded that the difference of buffer leakage current is essential to determine the difference of breakdown voltage here.

It should be noted that for power switch application, rather long L_{GD} such as ~10 μm is used. In such a case, the breakdown voltage is thought to increase significantly because the electric field profiles between the gate and the drain become rather uniform when the high-k dielectric is used. To evaluate the breakdown voltage for long L_{GD} is an important task yet to be done.

V. Conclusion

A 2-D analysis of breakdown characteristics of field-plate AlGaN/GaN HEMTs with a high-k passivation layer has been performed, and the results have been compared with those having a normal SiN passivation layer. As a result, it has been shown that the breakdown voltage is enhanced particularly in the cases with relatively short field plates, because the reduction in the electric field at the drain edge of gate effectively improves the breakdown voltage in the case with the high-k passivation layer. It has been also shown that in the case with moderate-length field plate, the breakdown voltage is enhanced for the case with the high-k passivation layer because the electric field profiles between the field-plate edge and the drain become more uniform. It has also been studied how the breakdown voltage depends on the deep-acceptor density in the Fe-doped semi-insulating buffer layer when a high-k passivation layer is used. It has been shown that the breakdown voltage increases with increasing the relative permittivity of the passivation layer ε_r and with increasing the deep-acceptor density N_{DA}. When $\varepsilon_r = 60$ and N_{DA} is 2–3 $\times 10^{17}$ cm^{-3} at a gate length of 0.3 μm, the breakdown voltage becomes about 500 V at a gate-to-drain distance of 1.5 μm, which corresponds to an average electric field of about 3.3 MV/cm between the gate and the drain.

We think that the techniques presented here such as the high-k passivation layer with a field plate and the high deep-acceptor density in the buffer layer can be used for power switch applications. However, when the high-k passivation layer with a field plate is applied to RF devices, the effects of parasitic capacitance on the frequency performance must be evaluated even if the field-plate length is short. Furthermore, even without a field plate, the fringing capacitance due to the high-k dielectric should be taken into consideration.

References

[1] U. K. Mishra, L. Shen, T. E. Kazior, and Y.-F. Wu, "GaN-based RF power devices and amplifiers," *Proc. IEEE*, vol. 96, no. 2, pp. 287–305, Feb. 2008.

[2] N. Ikeda *et al.*, "GaN power transistors on Si substrates for switching applications," *Proc. IEEE*, vol. 98, no. 7, pp. 1151–1161, Jul. 2010.

[3] A. Wakejima, K. Ota, K. Matsunaga, and M. Kuzuhara, "A GaAs-based field-modulating plate HFET with improved WCDMA peak-output-power characteristics," *IEEE Trans. Electron Devices*, vol. 50, no. 9, pp. 1983–1987, Sep. 2003.

[4] Y.-F. Wu *et al.*, "30-W/mm GaN HEMTs by field plate optimization," *IEEE Electron Device Lett.*, vol. 23, no. 3, pp. 117–119, Mar. 2004.

[5] Y. Hao *et al.*, "High-performance microwave gate-recessed AlGaN/AlN/GaN MOS-HEMT With 7% power-added efficiency," *IEEE Electron Device Lett.*, vol. 32, no. 5, pp. 626–628, May 2011.

[6] K. Horio, A. Nakajima, and K. Itagaki, "Analysis of field-plate effects on buffer-related lag phenomena and current collapse in GaN MESFETs and AlGaN/GaN HEMTs," *Semicond. Sci. Technol.*, vol. 24, no. 8, pp. 085022-1–085022-7, Aug. 2009.

[7] K. Horio, T. Tanaka, K. Itagaki, and A. Nakajima, "Two-dimensional analysis of field-plate effects on surface-state-related current transients and power slump in GaAs FETs," *IEEE Trans. Electron Devices*, vol. 58, no. 3, pp. 698–703, Mar. 2011.

[8] S. Karmalkar and U. K. Mishra, "Enhancement of breakdown voltage in AlGaN/GaN high electron mobility transistors using a field plate," *IEEE Trans. Electron Devices*, vol. 48, no. 8, pp. 1515–1521, Aug. 2001.

[9] E. Bahat-Treidel, O. Hilt, F. Brunner, V. Sidorov, J. Würfl, and G. Tränkle, "AlGaN/GaN/AlGaN DH-HEMTs breakdown voltage enhancement using multiple grating field plates (MGFPs)," *IEEE Trans. Electron Devices*, vol. 57, no. 6, pp. 1208–1216, Jun. 2010.

[10] H. Onodera and K. Horio, "Analysis of buffer-impurity and field-plate effects on breakdown characteristics in small-sized AlGaN/GaN high electron mobility transistors," *Semicond. Sci. Technol.*, vol. 27, no. 8, pp. 085016-1–085016-6, Aug. 2012.

[11] Q. Luo and Q. Yu, "Electric field modulation by introducing a HK dielectric film of tens of nanometers in AlGaN/GaN HEMT," *Nanosci. Nanotechnol. Lett.*, vol. 4, no. 9, pp. 936–939, 2012.

[12] H. Hanawa and K. Horio, "Increase in breakdown voltage of AlGaN/GaN HEMTs with a high-*k* dielectric layer," *Phys. Status Solidi A*, vol. 211, no. 4, pp. 784–787, 2014.

[13] H. Hanawa, H. Onodera, A. Nakajima, and K. Horio, "Numerical analysis of breakdown voltage enhancement in AlGaN/GaN HEMTs with a high-*k* passivation layer," *IEEE Trans. Electron Devices*, vol. 61, no. 3, pp. 769–775, Mar. 2014.

[14] C. Liu, E. F. Chor, and L. S. Tan, "Enhanced device performance of AlGaN/GaN HEMTs using HfO_2 high-*k* dielectric for surface passivation and gate oxide," *Semicond. Sci. Technol.*, vol. 22, no. 5, pp. 522–527, 2007.

[15] S. Yang *et al.*, "AlGaN/GaN MISHEMTs with high-*k* $LaLuO_3$ gate dielectric," *IEEE Electron Device Lett.*, vol. 33, no. 7, pp. 979–981, Jul. 2012.

[16] C.-S. Lee *et al.*, "Investigations of TiO_2–AlGaN/GaN/Si-passivated HFETs and MOS-HFETs using ultrasonic spray pyrolysis deposition," *IEEE Trans. Electron Devices*, vol. 62, no. 5, pp. 1460–1466, May 2015.

[17] H. Hanawa, Y. Satoh, and K. Horio, "Effects of buffer leakage current on breakdown characteristics in AlGaN/GaN HEMTs with a high-*k* passivation layer," *Microelectron. Eng.*, vol. 147, pp. 96–99, Nov. 2015.

[18] K. Horio and A. Wakabayashi, "Numerical analysis of surface-state effects on kink phenomena of GaAs MESFETs," *IEEE Trans. Electron Devices*, vol. 47, no. 12, pp. 2270–2276, Dec. 2000.

[19] K. Horio, K. Yonemoto, H. Takayanagi, and H. Nakano, "Physics-based simulation of buffer-trapping effects on slow current transients and current collapse in GaN field effect transistors," *J. Appl. Phys.*, vol. 98, no. 12, pp. 124502-1–124502-7, Dec. 2005.

[20] K. Horio and A. Nakajima, "Physical mechanism of buffer-related current transients and current slump in AlGaN/GaN high electron mobility transistors," *Jpn. J. Appl. Phys.*, vol. 47, no. 5R, pp. 3428–3433, 2008, doi: 10.1143/JJAP.47.3428.

[21] K. Horio, H. Onodera, and A. Nakajima, "Analysis of backside-electrode and gate-field-plate effects on buffer-related current collapse in AlGaN/GaN high electron mobility transistors," *J. Appl. Phys.*, vol. 109, no. 11, pp. 114508-1–114508-7, Jun. 2011.

[22] M. J. Uren *et al.*, "Punch-through in short-channel AlGaN/GaN HFETs," *IEEE Trans. Electron Devices*, vol. 53, no. 2, pp. 395–398, Feb. 2006.

[23] M. Silvestri, M. J. Uren, and M. Kuball, "Iron-induced deep-level acceptor center in GaN/AlGaN high electron mobility transistors: Energy level and cross section," *Appl. Phys. Lett.*, vol. 102, no. 4, pp. 073051-1–073051-4, 2013.

[24] Y. S. Puzyrev, R. D. Schrimpf, D. M. Fleetwood, and S. T. Pantelides, "Role of Fe impurity complexes in the degradation of GaN/AlGaN high-electron-mobility transistors," *Appl. Phys. Lett.*, vol. 106, no. 5, pp. 053505-1–053505-4, 2015.

[25] Y. Mitani, D. Kasai, and K. Horio, "Analysis of surface-state and impact-ionization effects on breakdown characteristics and gate-lag phenomena in narrowly recessed gate GaAs FETs," *IEEE Trans. Electron Devices*, vol. 50, no. 2, pp. 285–291, Feb. 2003.

[26] C. Bulutay, "Electron initiated impact ionization in AlGaN alloys," *Semicond. Sci. Technol.*, vol. 17, no. 10, pp. 59–62, 2002.

[27] R. Tsurumaki, N. Noda, and K. Horio, "Similarities of lag phenomena and current collapse in field-plate AlGaN/GaN HEMTs with different types of buffer layers," *Microelectron. Rel.*, vol. 73, pp. 36–41, Jun. 2017.

[28] Y. Kawada, H. Hanawa, and K. Horio, "Effects of acceptors in a Fe-doped buffer layer on breakdown characteristics of AlGaN/GaN high electron mobility transistors with a high-*k* passivation layer," *Jpn J. Appl. Phys.*, vol. 56, no. 10, pp. 108003-1–108003-3, 2017.

[29] Y. Saito, R. Tsurumaki, N. Noda, and K. Horio, "Analysis of reduction in lag phenomena and current collapse in field-plate AlGaN/GaN HEMTs with high acceptor density in a buffer layer," *IEEE Trans. Device Mater. Rel.*, vol. 18, no. 1, pp. 46–53, Mar. 2018.

Authors' photographs and biographies not available at the time of publication.